3D-QSAR and Molecular Mechanics Study for the Differences in the Azole Activity against Yeastlike and Filamentous Fungi and Their Relation to P450DM Inhibition. 1. 3-Substituted-4(3H)-quinazolinones

Filip Fratev* and Emilio Benfenati

Istituto di Ricerche Farmacologiche "Mario Negri", Via Eritrea, 62, 20157 Milano, Italy

Received November 22, 2004

A combination between 3D-QSAR and molecular mechanics (MM)-docking study was used as a tool to detail and model the mechanism of action of 46 antifungal azoles. Two methods of alignment of the ligands were performed: (i) alignment of the main skeleton without substituents and (ii) alignment of a defined substructure. The best model is characterized by q^2 with the values of 0.70 for yeastlike (yeast), 0.66 for filamentous fungi, and 0.70 for the selectivity against filamentous fungi. 3D-QSAR regression maps derived from six models were used to identify the regions responsible for the differences in the compounds activity against yeast and filamentous fungi. The binding energy of the important substructures (Local Binding Energy-LBE) and its standard deviation were calculated in order to demonstrate quantitatively the contribution of substituents reflecting the diversity of the antifungal activity. The comparisons of these results with the same regions of the contour maps indicated a good correspondence between the 3D-QSAR and MM (LBE) approaches allowing association between the maps and the participating residues in the active sites of P450DM of *C. albicans* and *A. fumigatus*. The $\pi-\pi$ interactions of two or more aromatic groups of the ligands with Phe228 and Tyr132 prove to be most important for the differences in activity against *C. albicans*. In *A. fumigatus* there was a better occupation of the inner central I-spiral in the areas around the heme. For the activity against *A. fumigatus* the $\pi-\pi$ interactions of aromatic groups of the compounds with Phe509, Phe228, and Tyr132 are significant for the activity.

INTRODUCTION

Yeastlike (yeast) and filamentous fungi cause between 80% and 90% of the fungal infections that have been treated with azole compounds for many years.[1−3] There are many reports of systematic searches for new ligands.[4−7] However, the difficulties in these studies are related to the design of compounds with high activity against filamentous fungi.[8,9]

The mechanism of action of the triazole antifungals involves the inhibition of the natural substrate lanosterol binding to P450DM (CYP51) through coordinating their triazole N4 atom to the sixth coordination position of the heme iron atom. The differences in the residues of CYP51 of *Candida albicans* and *Aspergillus fumigatus* and their relation to the ligand−protein interactions[10,11] has been used to explain the selectivity of fluconazol and other agents to these fungi.[12,13]

The 3D-models of *Candida albicans* CYP51 based on the homology models with X-ray template of other P450 members are available.[14−17] A number of 3D-QSAR and docking analysis was done[17−19] for a series of antifungal azoles with *Candida albicans* activity data, specifying some important ligand−enzymes interactions. In the present study, we focus on filamentous fungi (in particular *Aspergillus fumigatus*), the differences in the activity against yeast and filamentous fungi and their relation to the inhibition of CYP51. We used the combination of 3D-QSAR analysis and molecular mechanics binding energy calculation in the active site of *Candida albicans* and *Aspergillus fumigatus* to detail and model the differences in the azole-CYP51 complexes. Our methodology combines the computational approaches applied here. For this purpose we modified some methods and descriptors.

The ligand−receptor binding energy is the descriptor normally utilized for correlation with biological activity.[20] In the present paper we transformed this formulation for the substructures of the ligands involved in the ligand−enzymes interactions, and we calculated their local binding energy (LBE).

The "structure-based 3D-QSAR" approach is a common adopted combination of the 3D-QSAR and docking analysis.[21] The molecular mechanics optimization of the ligand−receptor complex after the preliminary docking procedure is often applied in this methodology and achieves more precision in the selection of the ligand conformation.[22] The next step is the compounds alignment using the obtained and optimized docking lowest energy conformers. However, when the experimental data are measured as a geometric means of "in vitro" values from different species (i.e. mix of various receptors data) this 3D-QSAR alignment is not applicable. In this study, we try to link and discuss below the combination between 3D-QSAR and MM-docking approaches without the use of docking conformers for the classes of yeast and filamentous fungi.

* Corresponding author phone: +39-02-39014499; fax: +39-02-39001916; e-mail: fratev@marionegri.it.

10.1021/ci0496494 CCC: $30.25
Published on Web 04/20/2005

Table 1. 3D-QSAR Results for Training Set Compounds

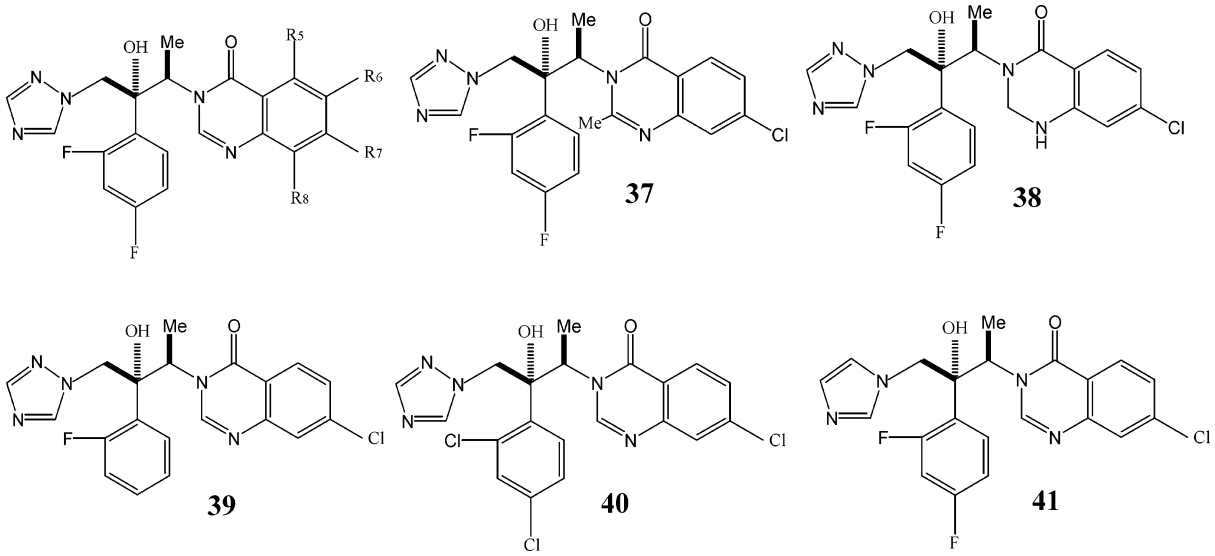

					RA(*yy*)[a]			RA(*ff*)[b]			RA(*ff*/*yy*)[c]		
N[d]	R5	R6	R7	R8	exp[e]	pre[f]	res[g]	exp	pre	res	exp	pre	res
1					1.07	1.11	−0.04	−0.30	−0.34	0.04	−1.37	−1.42	0.05
2	H	H	H	H	0.54	0.55	−0.01	0.35	0.22	0.13	−0.19	−0.28	0.09
3	Cl	H	H	H	0.16	0.14	0.02	−0.52	−0.52	0.00	−0.68	−0.67	−0.01
4	H	Cl	H	H	0.65	0.50	0.15	−0.37	−0.36	−0.01	−1.02	−0.95	−0.07
5	H	H	Cl	H	1.18	0.95	0.23	1.49	1.29	0.20	0.31	0.28	0.03
6	H	H	H	Cl	0.26	0.28	−0.02	−0.32	−0.38	0.06	−0.58	−0.58	0.00
7	F	H	H	H	0.00	0.06	−0.06	−0.44	−0.34	−0.10	−0.44	−0.36	−0.08
8	H	F	H	H	0.26	0.33	−0.07	<−0.53	NA[h]	NA	NA	NA	NA
9	H	H	F	H	0.68	0.57	0.11	0.92	0.58	0.34	0.24	0.09	0.15
10	H	Br	H	H	0.49	0.55	−0.06	−0.28	−0.39	0.11	−0.77	−0.91	0.14
11	H	H	Br	H	1.10	1.11	−0.01	1.47	1.55	−0.08	0.38	0.44	−0.06
12	H	F	F	H	0.43	0.42	0.01	−0.51	−0.35	−0.16	−0.94	−0.86	−0.08
13	H	Cl	H	Cl	0.46	0.39	0.07	<−0.53	NA	NA	NA	NA	NA
14	H	Br	H	Br	0.35	0.46	−0.11	<−0.53	NA	NA	NA	NA	NA
15	Me	H	H	H	0.22	0.28	−0.06	−0.29	−0.21	−0.08	−0.51	−0.47	−0.04
16	H	Me	H	H	0.49	0.49	0.00	−0.34	−0.20	−0.14	−0.83	−0.74	−0.09
17	H	H	H	Me	0.27	0.24	0.03	−0.59	−0.60	0.01	−0.86	−0.86	0.00
18	H	Me	H	Me	0.07	0.13	−0.06	<−0.53	NA	NA	NA	NA	NA
19	H	Me	H	Br	0.39	0.23	0.16	<−0.53	NA	NA	NA	NA	NA
20	H	H	H	OMe	−0.35	−0.35	0.00	<−0.53	NA	NA	NA	NA	NA
21	H	OMe	OMe	H	−0.20	−0.21	0.01	−0.54	−0.56	0.02	−0.34	−0.34	0.00
22	H	F	NMe_2	H	0.53	0.50	0.03	0.02	0.07	−0.05	−0.52	−0.47	−0.05
23	H	F	NH_2	H	−0.29	−0.12	−0.17	−0.37	−0.27	−0.10	−0.08	−0.09	0.01
24	H	F	$NHCOCF_3$	H	−0.17	−0.19	0.02	−0.48	−0.50	0.02	−0.32	−0.37	0.05
25	H	H	I	H	1.26	1.36	−0.10	1.46	1.61	−0.15	0.20	0.22	−0.02
26	H	H	CN	H	0.74	0.84	−0.10	0.78	0.84	−0.06	0.04	0.02	0.02
27	H	H	CF_3	H	0.84	0.89	−0.05	1.02	1.09	−0.07	0.18	0.13	0.05
28	H	H	OCH_2CH_2F	H	0.55	0.59	−0.04	−0.07	−0.16	0.09	−0.62	−0.62	0.00
29	H	H	OCH_2CHF_2	H	0.56	0.55	0.01	−0.01	−0.02	0.01	−0.57	−0.61	0.04
30	H	H	OCH_2CF_3	H	0.73	0.72	0.01	0.23	0.27	−0.04	−0.50	−0.47	−0.03
31	H	H	$OCH_2CF_2CHF_2$	H	1.14	1.10	0.04	0.17	0.05	0.12	−0.97	−1.03	0.06
32	H	H	SMe	H	0.97	1.02	−0.05	0.77	0.78	−0.01	−0.20	−0.24	0.04
33	H	H	SPh	H	0.88	0.92	−0.04	1.10	1.13	−0.03	0.22	0.29	−0.07
34	H	H	O−(p-ClPh)	H	0.89	0.92	−0.03	0.57	0.62	−0.05	−0.33	−0.27	−0.06
35	H	H	NHBn	H	0.64	0.63	0.01	0.36	0.37	−0.01	−0.28	−0.30	0.02
36	H	H	NMe_2	H	0.54	0.56	−0.02	−0.52	−0.46	−0.06	−1.06	−0.99	−0.07
37					−0.15	−0.17	0.02	−0.21	−0.23	0.02	−0.06	0.03	−0.03
38					0.75	0.68	0.07	0.89	0.80	0.09	0.14	0.15	−0.01
39					0.79	0.75	0.04	1.27	1.33	−0.06	0.48	0.45	0.03
40					0.37	0.30	0.07	−0.10	−0.09	−0.01	−0.47	−0.49	0.02

[a−c] Relative activity against yeast, filamentous fungi, and their ratio, respectively. [d] Compounds number. [e] Experimental activity. [f] Predicted activity by 3D-QSAR. [g] Differences between experimental and predicted by 3D-QSAR. [h] Not available data.

MATERIALS AND METHODS

Biological Data. Tables 1 and 2 show a series of antifungal 3-substituted-4 (3H)-quinazolinones, which were divided in to a training set and a test set. In the text here, we referred to the common 2,4 F phenyl ring as a ring 1, to the condensed phenyl ring in the quinazolinone structure as a ring 2, and to the pyrimidine ring in the quinazolinone structure as a ring 3. The training set consists of 40 and 34 compounds for yeast and filamentous fungi, respectively. The test set comprises five compounds covering a wide range of biologi-

Table 2. 3D-QSAR Results for Test Set Compounds

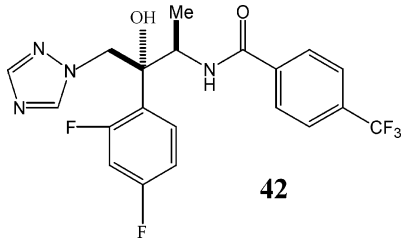

42

					RA(*yy*)[a]			RA(*ff*)[b]			RA(*ff/yy*)[c]		
N[d]	R5	R6	R7	R8	exp[e]	pre [f]	res	exp	pre	res	exp	pre	res
41					1.39	1.36	0.03	1.16	1.18	−0.02	−0.25	−0.22	−0.03
42					0.00	−0.04	0.04	0.00	−0.09	0.09	0.00	0.12	−0.12
43	H	H	1-triazolyl	H	−0.13	−0.05	−0.08	−0.54	−0.56	0.02	−0.47	−0.40	−0.07
44	H	H	2-tetrazolyl	H	0.51	0.36	0.15	−0.39	−0.47	0.08	−0.81	−0.90	0.09
45	H	H	morpholine	H	0.42	0.39	0.03	−0.16	−0.21	0.05	−0.65	−0.59	−0.06

[a] −*g*See the corresponding footnotes in Table 1.

cal data and the structural diversity of the compounds in the training set.

Geometric means of the individual minimum inhibitory concentrations (MIC) against six filamentous fungi (MIC(*ff*)) and 10 yeasts (MIC(*yy*)) were taken from ref 9. The (MIC) was defined as the lowest concentration (μg/mL) of a tested substance at which there is no macroscopic colonial growth in comparison with a blank experiment after the present incubation time. The yeast class included the following: *Candida albicans 60*; *Candida albicans 406*; *Candida albicans 76*; *Candida guilliermondii 26*; *Candida krusei 70*; *Candida parapsilosis 61*; *Candida pseudotropicalis 13*; *Candida tropicalis 2.11*; *Rhodotorula rubra 16*; *and Torulopsis glabrata 78*.

The group of filamentous fungi included the following*: Aspergillus flavus 19; Aspergillus fumigatus 33; Aspergillus niger 18; Microsporum canis 47; Microsporum gypseum 22; Trichophyton mentagrophytes 23; and Trichophyton rubrum 90.*

In this paper the antifungal activity presented in logarithm units log RA(*yy,ff)* was compared to compound 42 (Sankyo's amido alcohol[23]) and estimated using the following equation

$$\mathrm{RA}(yy,ff) = \mathrm{MIC}\ (42)\cdot\mathrm{MW(x)}/\mathrm{MIC(x)}\cdot\mathrm{MW}(42) \quad (1)$$

where RA is the relative activity, MIC(42), MW(42), MIC(x), and MW(x) are the (MIC) and the molecular weight of compound 42, and the corresponding ligand X from the series. To obtain information on the selectivity against filamentous fungi we used the equation

$$\mathrm{RA}(ff/yy) = \mathrm{Log}\ [\mathrm{RA}(ff)/\mathrm{RA}(yy)] \quad (2)$$

where RA(*ff*) and RA(*yy*) were calculated by eq 1.

Model of Molecules. We constructed 3D-models with the help of the standard HyperChem library.[24] Conformational analysis was done using molecular mechanic simulations under AM1 Hamiltonian.[25] The compounds were heated for 2 ps to 700 K and then ran for 5 ps to 310 K. After 2 ps three low-conformers were selected, and after geometry optimization (AM1 method) by a high "conjugate" gradient criterion value of 0.01 kcal/mol/Å, the lower energy conformation was chosen.

3D-QSAR METHOD

We generated electrostatic and van der Waals (VdW) volume maps for each compound. The electrostatic potentials and VdW volume distributions were obtained in different points of a virtual grid. Further, the compounds were aligned, and then the map descriptors were calculated. The 3D-QSAR alignment and map descriptors calculations were done using Chem-X software.[26]

Alignment of Molecules. The alignment of compounds was based on earlier reports about coordination of similar antifungal azoles to the iron atom of the heme[27,28] and previous 3D-QSAR studies.[29] We applied two patterns of superposition. In the first one were used all heavy atoms (C, N, etc. atoms but not H) of the compounds except those of the substituents in ring 2 (model 1). In the second model we eliminated ring 2 as well as the C and N atoms of the first and second positions in the ring 3. The molecules were aligned according to these two models by rigid fitting using least-squares fitting algorithm.[30]

3D-QSAR-Map Descriptors Calculation and Models Generation. The constructed grid possesses automatically determined dimensions and density, one point per Å. The electrostatic descriptors were generated by unit positive charge, and for steric descriptors we used the value of van der Waals volume for each grid point (VdW volume maps); the energy cutoff for electrostatic potentials was 20 kcal/mol. For 3D-QSAR maps interpretation, we utilized individual models including steric or electrostatic map descriptors and applied partial least-squares (PLS) analysis for the statistical calculations.[31] As a consequence, we used individual steric and electrostatic cross-validations (leave-one-out procedure) expressed by q^2s, q^2e and regression coefficients expressed by r^2s, r^2e. When both steric and electrostatic descriptors are involved these coefficients are symbolized as q^2 and r^2. Using from 1 to 10 components we generated 10 individual conventional 3D-QSAR models for compounds of the training set. Applying a cross-validation procedure we estimated the standard error of prediction (E cross) of each model and then obtained the optimal number of

components according to the criteria for the least value of E cross. This method has been reported frequently.[32] Further, the test set was used to estimate the predictive ability of the models.

MOLECULAR MECHANIC ANALYSIS OF THE LIGAND−ENZYME COMPLEXES

The homology models for P450 of *C. albicans* based on the bacterial P450BM-3, P450terp, and P450eryF crystal structures and the model for the amino acids sequence alignment between CYP51 *C. albicans* and *A. fumigatus* were taken from literature.[17,33] The residue numbers for both cytochromes follow the numeration from the sequence of *C. albicans* as in ref 17. We do not profit from the *Mycobacterium tuberculosis* CYP51 crystal structure[34] for homology modeling by some specific reasons. First, one of our main targets is to compare the results from molecular mechanics approaches used here to the other CYP51 *C. albicans* docking studies. The investigations reported by the time of our calculations were based on the homology modeling with bacterial crystal structures, and for this reason we used the same information. The second point is related to our aim to establish the differences between *C. albicans* and *A. fumigatus*, and we need to compare our results to the previous model for *C. albicans*.

We designed our 3D-model upon coordinates transferred directly from P450BM-3[35] for the main chain. The other residues were constructed again. They were optimized by AMBER 96[36] force field, step-dependent gradient up to 1 kcal/mol/Å, and "Conjugate" gradient up to 0.01 kcal/mol/Å. The charges were calculated by the Gasteiger−Marsili method.[37]

As a starting point in the molecular mechanic optimization we coordinated the triazole N4 atom with the Fe atom of the heme at the constant distance of 2.043 Å and an orientation to the Cys residue, taken from crystallographic studies.[38] The most favorable position for the azole−enzyme complex was found by rotating the N4−Fe bond 360° in 10° steps. The binding energies were found by molecular mechanic optimization on both enzyme and the compound by AMBER 96 over these 36 positions (36 ligand−enzyme complexes) with a criterion for the gradient of 0.01 kcal/mol/Å. For each compound, we chose the lowest binding energy, estimated by the equation

$$\text{E binding} = \text{E complex} - (\text{E ligand} + \text{E receptor}) \quad (3)$$

where E ligand, E receptor, and E complex are the energy of the ligand, the enzyme, and its complex, respectively. For the lowest energy ligand−enzyme complexes, we calculated the partial electrostatic and steric local binding energies (LBE) contributed by rings 1, 2, and 3, which was the binding energy only for these rings. The same calculation procedure was applied for some of the substituents in ring 2. For LBE assessment we used the following approximations

$$\text{E ebind} = \text{E°e ligand} - \text{Ee ligand} \quad (4a)$$

$$\text{E sbind} = \text{E°s ligand} - \text{E s ligand} \quad (4b)$$

where E ebind is the electrostatic binding energy that is calculated from the difference between the electrostatic energy of the ligand when it is bound to the enzyme (E°e ligand), compared to its electrostatic energy when it is not bound (Ee ligand). In a similar way we calculated E sbind, which is the steric LBE.

Table 3. Summarized PLS Results

	model l			model 2		
	RA(*yy*)	RA(*ff*)	RA(*ff/yy*)	RA(*yy*)	RA(*ff*)	RA(*ff/yy*)
NC[a]	40	34	34	40	34	34
q^2 [b]	0.658	0.700	0.713	0.656	0.699	0.697
OC	8	7	8	7	7	8
r^2	0.935	0.954	0.955	0.966	0.978	0.983
F	60.2	77.6	66.1	130.0	161.6	184.6
q^2e[c]	0.780	0.684	0.482	0.784	0.735	0.569
OCe	7	8	8	7	7	7
r^2e	0.921	0.927	0.891	0.963	0.954	0.929
*F*e	38.6	39.4	25.4	119.3	77.0	48.3
q^2s[d]	0.170	0.460	0.491	0.305	0.462	0.427
OCs	6	7	6	5	7	7
r^2s	0.782	0.883	0.801	0.837	0.884	0.934
*F*s	17.2	28.0	18.1	35.0	28.4	52.5

[a] Number of the compounds in 3D-QSAR model. [b] $-dq^2$, OC, r^2, and *F* are cross-validation regression coefficient, optimum number of components, regression coefficient, and Fisher criterion for the common (streric + electrostatic) 3D-QSAR model (rows 2 to 5), 3D-QSAR model using electrostatic descriptors (rows 6 to 9) and model with steric descriptors (rows 10 to 13).

RESULTS

3D-QSAR Models 1 and 2. Table 3 summarizes the PLS results for models 1 and 2. In both models with activities against yeast, the value of q^2 for electrostatic descriptors gave similar values using the same optimal number of components. However, the steric model 1 (see q^2s for RA(*yy*) in Table 3) gave a poor $q^2 = 0.17$, and in general the conventional r^2 gave better values in model 2. From these results it can be concluded that the ligand alignment of model 2 for yeast was performed better. For filamentous fungi and for the selectivity to filamentous we found a similar tendency (see Table 3): significantly better values for the r^2, statistical criteria (*F*-values), and better values for q^2, which prove the better quality of models 2. All subsequent calculations were therefore based on this model.

The alignment of compounds in the 3D-QSAR analyses indicates the possible binding location of the ligands in the activity site of the enzyme.[39,40] Models 2 showed the rigid binding state in the 3D-space of ring 1. These results are in agreement with a previous investigation.[29] Comparison of the PLS analysis with similar 3D-QSAR studies indicated that the models were improved by expanding the number of the heavy atoms used in the superposition.[29] Including rings 2 and 3 (model 1), however, showed significantly worse statistical indexes referring to their free orientation in the 3D-space. This is expressed well in the models with activity against yeast fungi. The torsion freedom of rings 2 and 3 is probably important for the differences in antifungal activity. The significance of the secondary aromatic rings orientation is supported by SAR study.[8]

3D-QSAR for the Activity against Yeast Fungi. We used 40 compounds for generating the 3D-QSAR model. Table 3 shows the results of PLS analysis. Comparison of the q^2s and q^2e values for the steric and electrostatic models indicated a little contribution of the van der Waals volume distribution. This was also seen from the less predictive ability (q^2 =

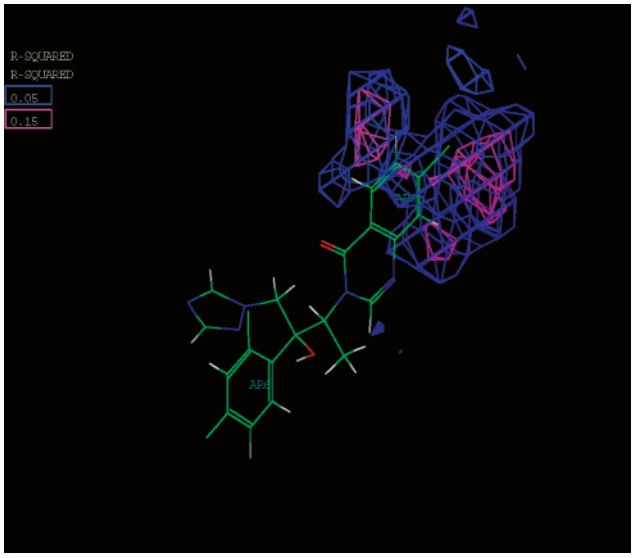

Figure 1. 3D-QSAR regression electrostatic contour map of activity against yeast fungi using ligand 5 for visualization. Regions with values of the regression coefficient squared (R^2) equal to 0.05 are colored in blue, while regions with R^2 values in the range of 0.15−0.5 in magenta.

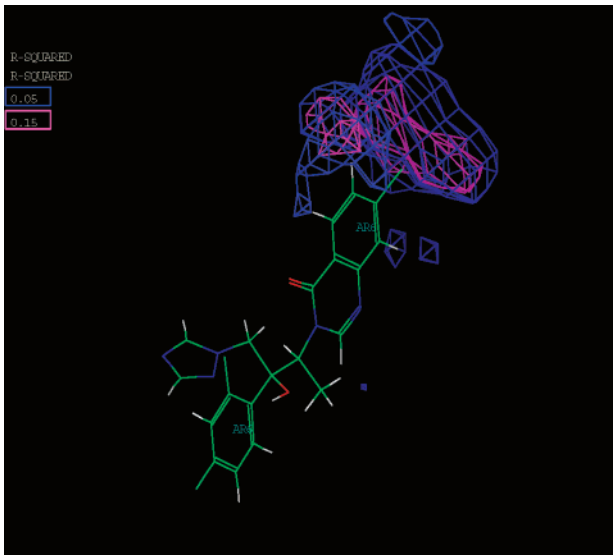

Figure 2. 3D-QSAR regression steric contour map of activity against yeast fungi using ligand 5 for visualization. Regions with values of the regression coefficient squared (R^2) equal to 0.05 are colored in blue, while regions with R^2 values in the range of 0.15−0.5 in magenta.

0.656) of the common model (i.e. the model with steric+ electrostatic descriptors) than the electrostatic one (q^2 = 0.784). The conventional model was constructed using seven optimal components and covered 96.6% of the antifungal activity diversity. The statistical results and predicted activity (see Tables 1 and 3) of the ligands illustrate the predictive ability of the model. The model is validated on test set compounds (Table 2). Figures 1 and 2 present regression 3D-QSAR contour maps derived from the steric and electrostatic models, indicating the important for the antifungal activity electrostatic and steric compounds regions. A blue contour shows the regions with regression levels toward the antifungal activity equal to R^2 = 0.05. The areas with a magenta contour correspond to the range of R^2 = 0.15−0.5.

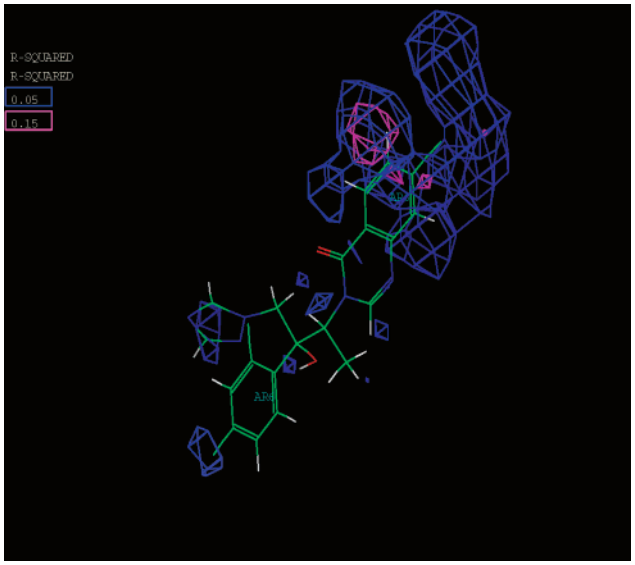

Figure 3. 3D-QSAR regression electrostatic contour map of activity against filamentous fungi using ligand 5 for visualization. Regions with values of the regression coefficient squared (R^2) equal to 0.05 are colored in blue, while regions with R^2 values in the range of 0.15−0.5 in magenta.

3D-QSAR for the Activity against Filamentous Fungi. We included 34 ligands in the 3D-QSAR investigation. PLS is a chemometric technique, which allows summarizing variables into components, related to a given amount of the parameter under study. In our case, the conventional model was constructed with seven components and covered 97.75% of the diversity in the antifungal activity. Tables 1 and 3 show predicted activity of each compound and the overall statistical results from PLS analysis. The cross-validation coefficient q^2 = 0.699 and the error E cross = 0.545 of the model showed high predictive ability. This was confirmed by results on the test set (Table 2). The small difference between the predicted and experimental values confirms the quality of the model. The tendency for a low contribution of the steric interactions also applies to filamentous fungi. Figures 3 and 4 present the regression contour maps for steric and electrostatic models. Their definition is equivalent in those in Figures 1 and 2.

3D-QSAR for the Ratio of Activities on Yeast and Filamentous Fungi. The predictive ability of the model was high, as indicated by the results for the test set (Table 2). The comparison of q^2 and r^2 values of the models with steric and electrostatic descriptors shows their similar contribution. In contrast to yeast and filamentous models, we obtained a significantly higher value of the common model (q^2 = 0.697) than in the individual ones. This can be explained with the similarity in the areas of ligands where these interactions are significant. Figures 5 and 6 present the regression maps of the regions significant, for the selectivity toward filamentous fungi. Their definition is equivalent in those in Figures 1 and 2.

Molecular Mechanics Analysis in the Active Site of P450DM of *C. albicans* and *A. fumigatus*. Figure 7 presents a view of compound 5 in the active site of P450 *C. albicans*. Met306 gives hydrogen bonds with Glu309 and Gly303, forming an original hydrogen bridge. The hydroxyl group of the ligands makes an H-bond with Met306. This indicates the importance of this group in a ligand−protein interaction.

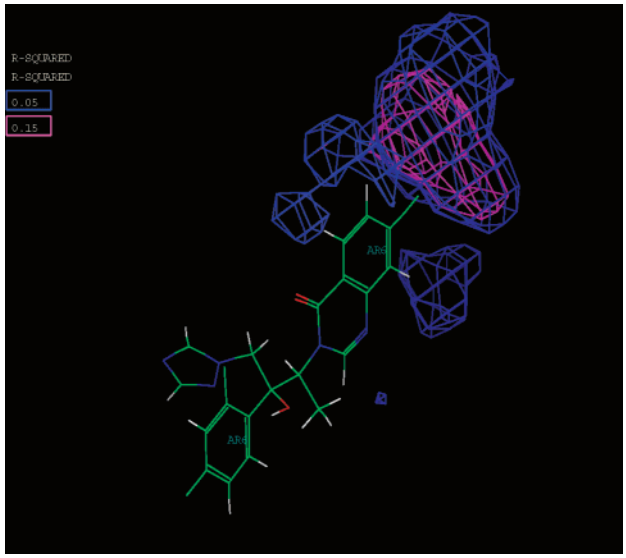

Figure 4. 3D-QSAR regression steric contour map of activity against filamentous fungi using ligand 5 for visualization. Regions with values of the regression coefficient squared (R^2) equal to 0.05 are colored in blue, while regions with R^2 values in the range of 0.15−0.5 in magenta.

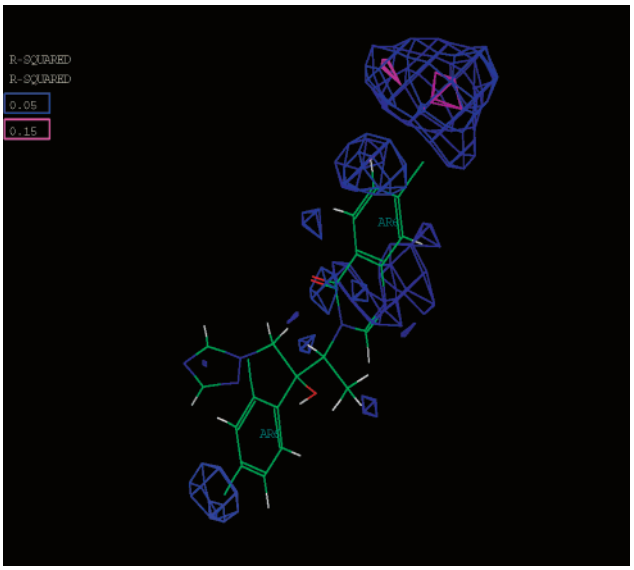

Figure 5. 3D-QSAR regression electrostatic contour map of ratio yeast/filamentous fungi using ligand 5 for visualization. Regions with values of the regression coefficient squared (R^2) equal to 0.05 are colored in blue, while regions with R^2 values in the range of 0.15−0.5 in magenta.

Furthermore, His310 is in close contact with the common carbonyl group. The important role of this residue has been discussed.[41−43] There is also an H-bond between Thr315 and Thr311. The last residue is in a close hydrophobic contact with ring 1 of the ligands. The role of Thr315 in the azole interactions in CYP51 of C. *albicans* was reported in a number of studies.[44−45] The mutation of Thr311 to Ala reduces the activity of compounds such as ketoconazole by up to 4−5 times.[46]

The main factors for both the orientation of molecules and the ligand−protein interactions are the hydrophobic and $\pi-\pi$ contacts of rings 2 and 3 with Phe228 and Tyr132. Ring 3, which has the same structure in all compounds, is in close contact with Thr132. The role of this residue in fluconazole resistance has been identified.[47,48] In previous studies the

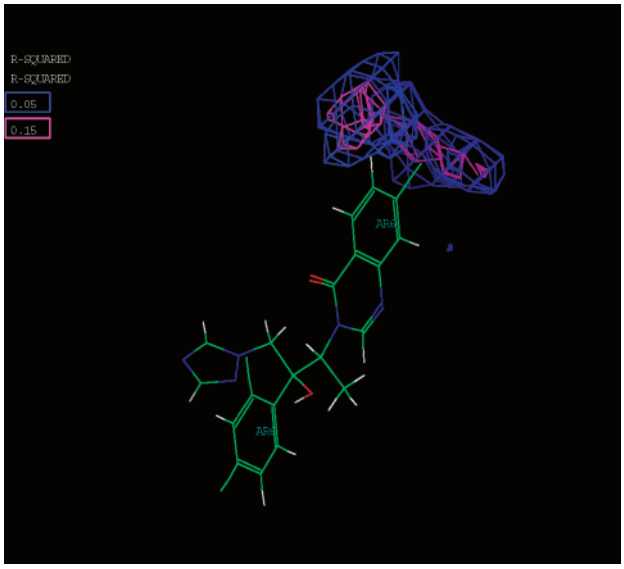

Figure 6. 3D-QSAR regression steric contour map of ratio yeast/filamentous fungi using ligand 5 for visualization. Regions with values of the regression coefficient squared (R^2) equal to 0.05 are colored in blue, while regions with R^2 values in the range of 0.15−0.5 in magenta.

same interactions were indicated for the halogenated phenyl ring (ring 1 here) and Tyr132 for fluconazole and other ligands.[17−19,49,50] In these studies there was only one aromatic ring in the side near to heme and modest activity.

In our case we have the quinazolinone ring as well and the activity is higher for many compounds. The interactions of two aromatic groups with Tyr132 and Phe228 are probably major factors for the higher and more homogeneous activity against *C. albicans* of the compounds in the series studied. We identify the hydrophobic contact of ring 2 with Gly227. Considering the possible mutation of Thr229 to Ala[33] this can be an additional support for the ring 2 importance in the ligand−enzyme interaction. The pharmacophore model of azole compounds showed the significance of the second phenyl ring too.[51]

Figure 8 presents ligand 5 in the activity site of P450DM of *A. fumigatus* (residues are numbered with *C. albicans* nomenclature). Ile315 forms an H-bond with Thr311, which is in close contact with ring 1 and makes an H-bond with a N (2) atom of a triazole ring. This original bridge explains why these residues are more important in the ligand−protein interaction in *A. fumigatus* than *C. albicans*.

An additional interaction was also observed at His310 and Glu309. The amino groups of these residues form hydrogen bonds with the fluorine atom on the second position in ring 1. There is a better occupation of the inside-long-central I-spiral in *A. fumigatus*. Ring 2 and part of ring 3 are in close contact, and $\pi-\pi$ interactions with Phe509 are stronger than in rings 1 and 3 with Tyr132. Thus, Tyr132 is less significant in *A. fumigatus*. In the immediate proximity of ring 2 is Phe228. Ring 2 $\pi-\pi$ interactions with Phe126 were observed for some compounds too.

Phe228, Phe126, and Tyr132 and the substitution of the selective residue Val509[17] with Phe509 in *A. fumigatus* and their interaction with rings 2 and 3 are important for the compounds activity.

In general, Phe and Tyr residues and their conformation greatly influence the conformation of the compounds in the

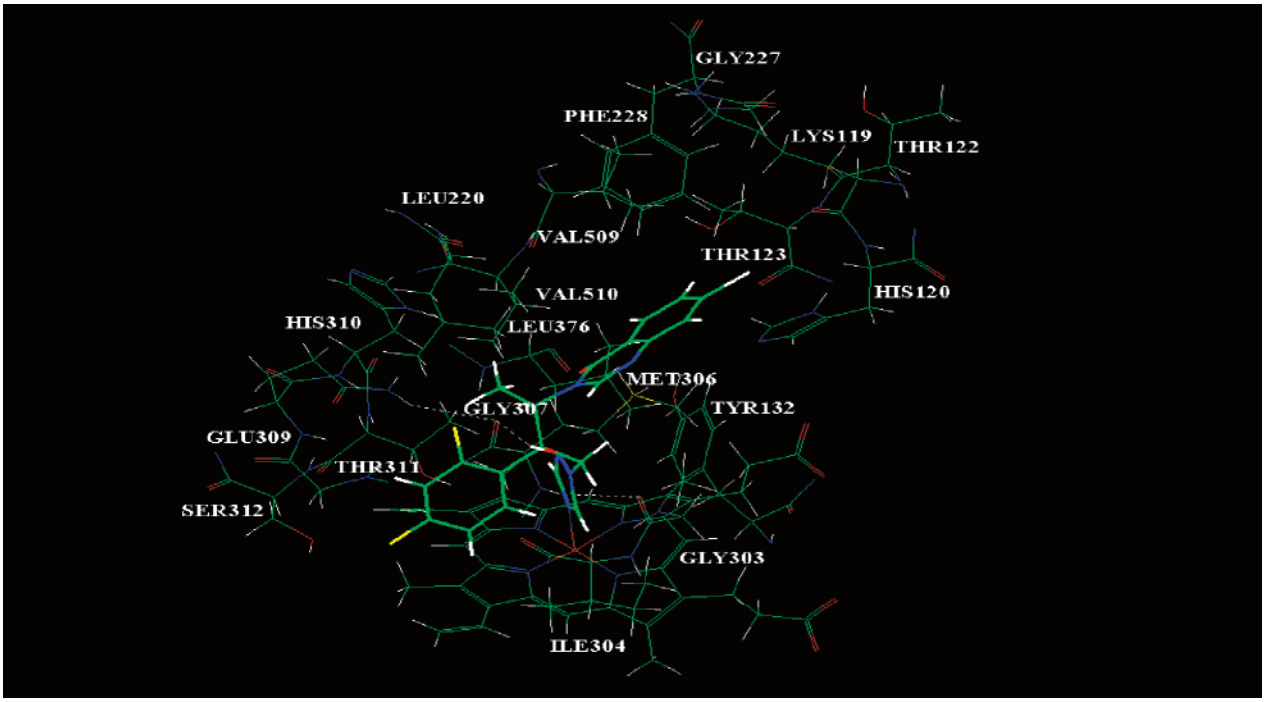

Figure 7. Docking view of compound 5 in the binding site of *C. albicanas*.

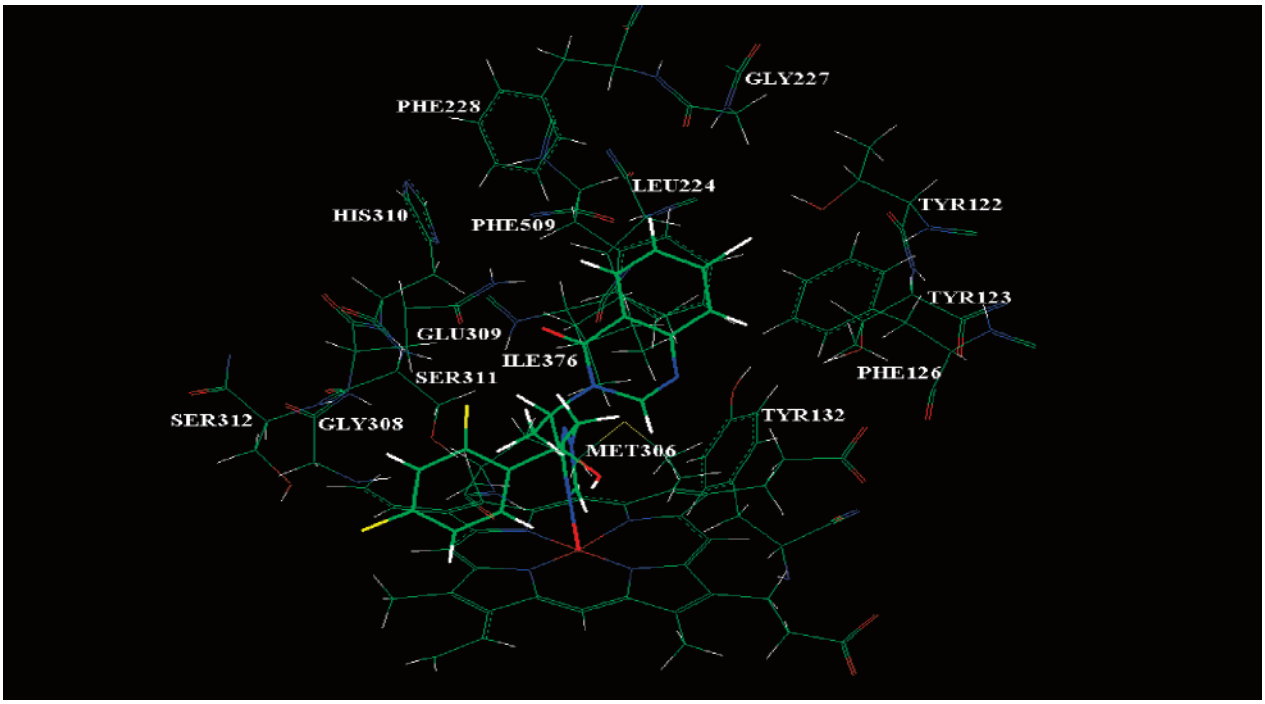

Figure 8. Docking view of compound 5 in the binding site of *A. fumigatus*.

P450 family. This was indicated by different techniques. The crystallographic data showed essential conformation changes in Phe87 and Tyr96 in P450cam.[38] In CYP51 from *Mycobacterium tuberculosis* aromatic groups of fluconazole and ketoconazole were in close contact with Phe and Tyr residues.[34] In CYP1 Phe and Tyr residues were defined for the accessibility of the heme areas in different heterocycle compounds.[52] Biochemical and microbiological analysis identified an important role of Phe233 and Phe235 for tetraconazole activity in *C. albicans*.[53] The phenotype resistances, which were important in *Saccharomyces cerevisiae*, reduce the biosynthesis of ergosterol from 4 times but increase the sensitivity to ketoconazole more than 200-fold.[54] This indicates a hypersensitivity to the alternative electron-transfer systems. Hence, the results from the present study regarding the importance of Phe228, Phe126, Tyr132, and Phe509 in ligand−protein interactions in *A. fumigatus* are not surprising and in agreement with the investigations cited above.

In addition, there is an apparent difference in the orientation of the aromatic rings in *C. albicans* and *A. fumigatus* (see Figures 7 and 8). The orientation of ring 1 was similar in the two types and the differences in the contacts with residues are due to the rotation of the ligands around the

N−Fe bond. In *A. fumigatus* rings 2 and 3 had less torsion freedom than in *C. albicans* probably because of the close contact with Phe509. The rotatability of these two rings is confirmation of the chosen alignment of the compounds for 3D-QSAR. The limitation of the rotation of rings 2 and 3 in the 3D-QSAR model 1 for *C. albicans* dramatically worsens its steric statistical parameters but not for *A. fumigatus* (see Table 3).

A Difference between Yeast and Filamentous Fungi Indicated by 3D-QSAR Maps. The main aim of this study was to obtain information about the differences in inhibition in yeast and filamentous fungi by azoles. The contour maps (Figures 1−6) from the 3D-QSAR investigation were used to compare the regions and substituents important for the differences in the activity.

Figure 1 presents the electrostatic regression contour map obtained from the 3D-QSAR model related to the activity against yeast fungi. The larger regions causing significant contribution (magenta contour) correspond to the R7 and R8 positions of ring 2 (see also Table 1). The region around the sixth position showed the same level of importance. These results identified the important substitutions in yeast fungi. The large blue regions which overlap the top part of ring 2 and also the magenta area around the C atom in position R7 probably reflect a contribution of the $\pi-\pi$ localization and $\pi-\pi$ interactions in ring 2 and/or its flexible position in the space. Regions around the second position in ring 3 and C (3) and N (4) atoms of the azole ring appeared to be less important for the differences in yeast activity. Ring 1 and the hydroxyl group did not contribute to the regression levels.

The map for steric interactions is presented in Figure 2, showing a large region between the R7 and R8 positions and a smaller one around the R6 position of ring 2. Figures 1 and 2 clearly show the greatest contribution of ring 2 to the differences in the inhibition activity against yeast fungi.

Figure 3 presents the contour map of the electrostatic interactions derived from the 3D-QSAR model related to activity against filamentous fungi. Substituents on the R6 position in ring 2 accounts for most of the differences from the yeast model. Magenta regions around C (7) and C (6) atoms of this ring are probably results from $\pi-\pi$-electron interactions. The same applies for the top parts of ring 3.

There are differences in the two models (yeast and filamentous) in the regions with a blue contour around ring 2. In Figure 1 they are on the left in the map, while in Figure 3 they are larger on the right. The areas (blue contour) around N (3) and N (1) atoms of ring 3 are not presented in the yeast model (Figure 1). Important for the differences in the activity against filamentous fungi were also the substituents on the second and fourth positions in ring 1 and the region around the hydroxyl group.

The comparison of the electrostatic to steric interactions (Figure 4) show significant differences in the regions around ring 2. The steric fields make the greatest contribution between the seventh and the eight positions of ring 2, compared to the sixth position in the electrostatic model (Figure 3). These differences are in agreement with the results of PLS analysis, discussed above, and add more details relative to the relevance of specific substituents.

The differences in the regions important for the inhibitory activity against yeast and filamentous fungi can be recognized from the electrostatic interactions mainly. Considering their large contribution in the final models, we can summarize them:

(i) Different regions with the most significant contribution to the differences in activity: for yeast these are substituents in the R7 and R8 positions of ring 2, for filamentous fungi in the R6 position.

(ii) High importance of ring 3 for filamentous but low for yeast.

(iii) No contribution from ring 1 and a common OH group in yeast.

Further confirmation of these findings comes from Figures 5 and 6, which show the regions relevant to the differences in the activity between yeast and filamentous fungi, obtained with the 3D-QSAR for the ratio of activities on yeast and filamentous fungi. In practice, these regions indicate the selectivity of the compound for filamentous fungi. In Figure 5 magenta and blue contour marks the regions mainly around the R6 and R7 positions in ring 2. Ring 2 is almost completely covered with blue contour areas except for a region of substitutions in the eighth position. Of special importance is the OH group and para position of ring 1. The steric interactions (Figure 6), due to the substituents on the sixth and seventh positions in ring 2, have the important role.

3D-QSAR and Molecular Mechanics Comparison. The 3D-QSAR contour maps show the regression values toward the activity of the ligands, in the regions with big standard deviation (SD) in electrostatic interactions and van der Waals volume distribution. Thus, the comparison of 3D-QSAR significant maps regions to the same ones from MM LBE SD and LBE regression toward the activity makes it is possible to compare the two methods. In the case of data collected as a geometrical mean from several "in vitro" experiments (in the present paper: 10 yeast and six filamentous) it was not possible using the docking conformers from one fungal CYP51 for the 3D-QSAR alignment.

Tables 4 and 5 present the binding energies and LBE of rings 1, 2, and 3 for compounds 5, 9, 12, 20, 21, and 28 in the active sites of *A. fumigatus* and *C. albicans*. In addition, for *A. fumigatus* the same energies were calculated also for ligands 10, 11, 15, 16, 22, and 23.

The steric and electrostatic binding energies in *C. albicans* were mostly lower than in *A. fumigatus*. As a whole ring 1 gave a weaker contribution than two other aromatic rings. The SD of the total binding energy (steric + electrostatic) for ring 1, ring 2, and ring 3 were respectively 1.83, 4.89, and 20.57 kcal/mol. Thus ring 2 contributes mostly to the ligand−protein differences in the interactions.

The comparison of these results with 3D-QSAR contour maps (Figures 1 and 2) leads to similar conclusions. Ring 1 is not involved in the differences of the activity, ring 3 gave a small contribution, and ring 2 is the most significant. The SD of electrostatic and steric binding energies at ring 2 are 17.88 and 3.42 kcal/mol, respectively. The much smaller contribution of the steric component is in agreement with the PLS results.

The LBE study of different substituents in the case of *C. albicans* resulted in the greatest deviation of electrostatic energies on the seventh position with SD 14.89 kcal/mol followed by the eighth and sixth one with SD 10.01 kcal/mol and SD 4.88 kcal/mol. The fifth position gave SD 1.98 kcal/mol. Thus, the biggest contribution to the differences

Table 4. Binding Energies and LBE (kcal/mol) in the Active Site of *A. fumigatus*

	compound numbers											
energy	**5**	**9**	**10**	**11**	**12**	**15**	**16**	**20**	**21**	**22**	**23**	**28**
Etot[a]	−137.5	−164.3	−155.11	−134.7	−179.1	−123.6	−136.22	−155.4	−187.7	−165.3	−174.1	−163.1
Ee	−74.7	−104.2	−94.44	−69.2	−120.3	−65.1	−75.18	−91.9	−119.9	−99.2	−110.1	−95.2
Es	−62.8	−60.1	−60.67	−65.6	−58.8	−58.6	−61.04	−63.5	−67.8	−66.2	−64.1	−67.9
E1tot[b]	−19.4	−35.0	−30.31	−18.0	−34.2	−18.1	−16.91	−16.7	−33.0	−8.4	−24.9	−21.2
E1e	−4.3	−22.5	−18.47	−2.8	−22.5	−6.2	−4.82	−4.1	−18.9	5.2	−9.6	−8.9
E1s	−15.1	−12.5	−11.84	−15.2	−11.7	−11.9	−12.09	−12.6	−14.1	−13.6	−15.3	−12.3
E2tot	−24.5	−23.6	−22.87	−26.8	−40.8	−42.7	−22.45	−50.9	−77.7	−45.9	−54.6	−51.5
E2e	−4.4	−5.1	−2.08	−3.9	−22.2	−19.6	−3.30	−28.4	−51.0	−25.8	−34.0	−24.8
E2s	−20.0	−18.5	−20.79	−22.9	−18.6	−23.0	−19.15	−22.4	−26.7	−20.1	−20.7	−26.7
E3tot	−44.8	−52.1	−50.42	−40.8	−55.5	−31.8	−38.49	−37.1	−22.7	−37.6	−44.6	−35.7
E3e	−30.3	−38.3	−37.48	−27.4	−42.5	−19.3	−25.28	−24.2	−9.9	−25.1	−30.7	−21.9
E3s	−14.6	−13.8	−12.94	−13.3	−13.1	−12.5	−13.21	−12.9	−12.8	−12.5	−13.9	−13.8
MIC(*ff*)[c]	0.7	2.5	45	0.8	70	40	45	>80	80	22	50	28

[a] Etot, Ee, and Es are the total (sum S+E), electrostatic, and steric binding energies for the compounds. [b] Similarly the other values are LBE for rings 1, 2, and 3, respectively. [c] MIC(*ff*) is minimum inhibitory concentrations (μg/mL) against *A. fumigatus*.[9]

Table 5. Binding Energies and LBE (kcal/mol) in the Active Site of *C. albicanas*

	compound numbers					
energy	**5**	**9**	**12**	**20**	**21**	**28**
Etot[a]	−145.9	−119	−163.2	−174.3	−198.2	−186.9
Ee	−81.9	−57.8	−100.9	−108.9	−129.2	−114.3
Es	−64.0	−61.2	−62.3	−65.4	−69.0	−72.5
E1tot[b]	−23.2	−24.5	−25.1	−25.6	−25.8	−21.0
E1e	−9.0	−8.6	−10.8	−11.0	−10.0	−6.0
E1s	−14.2	−15.9	−14.4	−14.6	−15.8	−15.0
E2tot	−20.0	−20.1	−36.7	−48.6	−71.3	−56.9
E2e	−1.8	−3.6	−19.6	−27.3	−48.9	−31.7
E2s	−18.2	−16.5	−17.1	−21.4	−22.4	−25.3
E3tot	−38.9	−31.1	−34.2	−42.8	−37.6	−43.8
E3e	−26.3	−17.4	−21.9	−31.8	−25.1	−30.6
E3s	−12.6	−13.6	−12.3	−11.0	−12.4	−13.2
MIC(*yy*)[c]	0.3	0.9	1.7	10	7.6	1.4

[a,b] See the corresponding footnotes in Table 4. [c] MIC(*yy*) is minimum inhibitory concentrations against *C. albicanas*.[9]

in these energies comes from the regions around the R7 and R8 positions in ring 2. Steric energies have the greatest deviation on the seventh and eighth positions with SD 17.07 and 3.04 kcal/mol, respectively, while for the sixth and fifth positions SD were 0.96 and 0.42 kcal/mol.

Looking at Figures 1 and 2 we can again find agreement between the 3D-QSAR and LBE methods. In addition, only for the LBE values on the R8 position we observed the statistical regression with activity on a level $\alpha = 0.09$ and $r = 0.76$, $p < 0.0807$, $n = 6$ for the electrostatic component and $\alpha = 0.09$, $r = 0.73$, $p < 0.853$, $n = 6$ for the steric one. In Figure 1 the magenta contours are very close only at this region of ring 2.

The 3D-QSAR regression maps derived from the model with activity against filamentous fungi (Figures 3 and 4) show the biggest contribution to the differences of the activity in ring 2, especially in the R6 place. Molecular mechanics energy calculations were in agreement with 3D-QSAR results. Standard deviations of the total LBE of rings 1, 2, and 3 were 8.77, 9.62, and 16.52 kcal/mol, respectively. These values are higher for the first two rings than the values calculated for *C. albicans*, as also seen in Figure 3: important for the differences in activity were electrostatic fields around the fourth position of ring 1 and a general enhancement of the significant regions around ring 3. The contribution to the SD of electrostatic and steric components in all aromatic groups was similar to *C. albicans*. For ring 2 we obtained SDe 14.81 and SDs 2.97 kcal/mol indicating the greater contribution of electrostatic interactions, in agreement with results from PLS analysis.

For electrostatic LBE at the fifth, sixth, seventh, and eighth positions of ring 2 the SD were 0.37, 5.12, 15.22, and 12.02 kcal/mol, respectively. They were obtained initially only with ligands 5, 9, 12, 20, 21, and 28. At position R6, there was a significant correlation at level $\alpha = 0.05$ with $r = 0.90$ and $p < 0.2436$, $n = 6$. Then we extended the number of compounds including ligands 11, 10, 15, 16, 22, and 23 (i.e. over 30% of the series). In this way, we included all type of substituents, covering the maximum range of the deviation at the R6 position. There was a significant regression toward activity only for this position. The level of significance was $\alpha = 0.05$, $r = 0.70$, t (9) = 3.3438, $p < 0.0086$, $n = 11$. There was also a similar correlation with the total and the electrostatic LBE of ring 2. Considering the influence of the different substituents on neighboring positions we can conclude that there is a close correspondence between the 3D-QSAR and molecular mechanics results. The important role of the substituents at the R6 position are probably linked to their close contact with Phe509 and Phe228 compared to other parts of ring 2 (see Figure 8).

DISCUSSION

In the present paper we used the bacterial homology model[17] to assess the precision on the molecular mechanics-docking methodology for searching the more realistic ligand position and identifying the important enzymes residues involved in the ligand−protein interaction; then we compared this model to the other docking models. During the preparation of our manuscript a new docking study for P450DM of *C. albicans* and *A. fumigatus* based on the homology modeling with *Mycobacterium tuberculosis* CYP51 crystal structure was published.[55] This was helpful because we can compare the results obtained from the different models.

The importance of the specific enzyme channel mentioned here surrounded by helix I, F, and β-strands $\beta1-4$, $\beta4-1$ was completely supported by the recently published docking analysis.[55] The interacting enzyme residues were the same or very similar to those we identified. Some changes in

residues contribution like Phe228 in our paper compared to Phe233 in ref 55 and also Leu508 for *A. fumigatus* compared to Phe509 are probably related to the large structural differences and especially to the location of the aromatic rings of posaconazole and compounds that we studied here. Comparison of these data with the previous results[17−19] shows similarity only in the predicted residues interaction at the areas near to the heme. One of the important differences was the indication of the significance on the Phe228-Phe233 region in our model and also in ref 55 in contrast to refs 17−19. The difference in the results from the same homology models allows concluding that the molecular mechanics optimization, both enzyme and the ligand approach used here, achieves better precision as compared to docking without of MM optimization. Additionally we provide a quantitative assessment on aromatic rings LBE showing that the long chains of the inhibitors are determining (as in ref 55) for activity and that in the most of the ligands the secondary rings are significant.

A mutual validation of the 3D-QSAR and docking approaches has been recommended and can reinforce the interpretation of SAR under investigation.[56] An example for this comparison was a complex of azoles and aromatic P450 (CYP17).[57] This model was obtained using a similar approach of molecular dynamic simulation and then molecular mechanic optimization, achieving 55% match between the coefficients on 11 points of the 3D-QSAR map and the corresponding steric energies points in the enzyme 3D space (the authors used only steric fields as a descriptors). In the present study, we applied the comparison for 3D-QSAR maps and the important parts of the compounds in a ligand−protein interaction presented quantitatively by their LBE and SD of the LBE values but not for individual points in the surrounding space. We used here 3D-QSAR regression maps, and for this reason we compared them to SD and regression of LBE values toward the activity. In contrast to the coefficient maps indicating quantitatively the positive or negative contribution of the areas around the ligands and comparable to the positive and negative energy in the enzyme,[57] the regression 3D-QSAR maps related to activity differences and their SD values in the different compounds regions.

The results presented here show a good match between all significant 3D-QSAR maps region with level in the range of $R^2 = 0.15-0.5$ and the corresponding LBE SD or regression values. Both 3D-QSAR and molecular mechanic simulation in the binding sites identified the residues significant for the differences between the studied fungi classes even if we used only one species of them (*C. albicans* and *A. fumigatus*) to obtain LBE values. An explanation of this fact is due to the identical enzymes residues involved in the ligand−complex interaction in the individual classes of yeast and filamentous fungi that form the final data for the 3D-QSAR studies. These results indicate that the use of the same alignment rules for the creation of models describing the activity toward several species avoids possible mistakes coming from the use of wrong docking conformers.

As a conclusion we can summarize that the 3D-QSAR models obtained here can be successfully applied in the search of new analogues of triazole compounds with better activity and selectivity for filamentous fungi. This process is supported by molecular mechanics LBE models, which show the important ligand−protein interactions and their differences in two of the most common fungi. We successfully combined 3D-QSAR and molecular mechanics techniques. The 3D-QSAR method and its modifications can build up useful statistical models for predicting the activity of the ligands. The docking analysis and molecular mechanics LBE calculation approach gives a good outline of the mechanism of action and could be helpful in finding new compounds. Using the molecular mechanic optimization in the enzymes active sites and LBE energy technique enabled us to test and interpret the 3D-QSAR models and contour maps, contributing to the identification of useful compounds on the basis of enzymes binding.

ACKNOWLEDGMENT

We gratefully acknowledge support for this research from the IMAGETOX EU Project (HPRN-CT-1999-00015). The authors thank to Dr. Irini Doytchinovafor Chem-X software and E. Mihaylova for the helpful discussions.

REFERENCES AND NOTES

(1) Richardson, K.; Brammer, K. W.; Marriott, M. S.; Troke, P. F. Activity of UK-49, 858, a bis-triazole derivative, against experimental infections with *Candida albicans* and *Trichophyton mentagrophytes*. *Antimicrob. Agents Chemother*. **1985**, *27*, 832−835.

(2) Borgers, M. In *The Scientific Basis of Antimicrobiol Chemotherapy*; Greenvood, D., Grady, F., Eds.; Cambridge University Press: Cambrige, 1985; p 133.

(3) Latge, J. *Aspergillus fumigatus and aspergillosis*. *Clin. Microbiol. Rev*. **1999**, *12*, 310−350.

(4) Warnock, D. W. Fungal infections in neutropenia: current problems and chemotherapeutic control. *J. Antimicrob. Chemother*. **1998**, *41*, 95−105.

(5) Konosu, T.; Takeda, N.; Tajima, Y.; Yasuda, H.; Oida, S. Synthesis and antifungal activities of some thiolane-triazole derivatives. *Chem. Pharm. Bull. (Tokyo)* **1990**, *38*, 1258−1265.

(6) Konosu, T.; Tajima, Y.; Takeda, N.; Miyaoka, T.; Kasahara, M.; Yasuda, H.; Oida, S. Triazole antifungals. II. Synthesis and antifungal activities of 3-acyl-4-methyloxazolidine derivatives. *Chem. Pharm. Bull. (Tokyo)* **1990**, *38*, 2476−2486.

(7) Tanaka, T.; Takeda, N.; Konosu, T.; Yasuda, H.; Oida, S. Triazole antifungals. V. Synthesis and antifungal activities of some amides related to 3-acylamino-2-aryl-1-triazolyl-2-butanol. *Chem. Pharm. Bull. (Tokyo)* **1992**, *40*, 661−665.

(8) Bartroli, J.; Turmo, E.; Algner, M.; Boncompte, E.; Vericant, M. L.; Coute, L.; Ramis, J.; Merlos, M.; Garica Rafanell, J.; Forn, J. New azole antifungals. 2. Synthesis and antifungal activity of heterocyclecarboxamide derivatives of 3-amino-2-aryl-1-azolyl-2-butanol. *J. Med. Chem.* **1998**, *41*, 1855−1868.

(9) Bartroli, J.; Turmo, E.; Algner, M.; Boncompte, E.; Vericant, M. L.; Coute, L.; Ramis, J.; Merlos, M.; Garica Rafanell, J.; Forn, J. New azole antifungals. 3. Synthesis and antifungal activity of 3-substituted-4 (3H)-quinazolinones. *J. Med. Chem*. **1998**, *41*, 1869−1882.

(10) Nelson, D. R.; Koymans, L.; Kamataki, T.; Stegeman, J. J.; Feyereisen, R.; Waxman, D. J.; Waterman, M. R.; Goton, O.; Goon, M. J.; Estabrook, R. W.; Gunsalus, I. C.; Nebert, D. W. P450 superfamily: update on new sequences, gene mapping, accession numbers and nomenclature. *Pharmacogenetics* **1996**, *6*, 1−42.

(11) Lai, M. H.; Kirsch, D. R. Nucleotide sequence of cytochrome P450 L1A1 (lanosterol 14 alpha-demethylase) from *Candida albicans*. *Nucleic Acids Res*. **1989**, *17*, 804.

(12) Denning, D. W.; Venkateswarlu, K.; Oakley, K. L.; Anderson, M. J.; Manning, N. J.; Stevens, D. A.; Warnock, D. W.; Kelly, S. L. Itraconazole resistance in *Aspergillus fumigatus*. *Antimicrob. Agents Chemother*. **1997**, *41*, 1364−1368.

(13) Sanglard, D.; Ischer, F.; Koymans, L.; Bille, J. Amino acid substitutions in the cytochrome P-450 lanosterol 14α-demethylase (CYP51A1) from azole-resistant *Candida albicans* clinical isolates contribute to resistance to azole antifungal agents. *Antimicrob. Agents Chemother*. **1998**, *42*, 241−245.

(14) Boscott, P. E.; Grant, G. H. Modelling cytochrome P450 14 alpha demethylase (*Candida albicans*) from P450cam. *J. Mol. Graph*. **1994**, *12*, 185−192.

(15) Sheng, C.; Zhang, W.; Zhang, M.; Song, Y.; Ji, H.; Zhu, J.; Yao, J.; Yu, J.; Yang, S.; Zhou, Y.; Zhu, J.; Lu, J. Homology modelling of lanosterol 14alpha-demethylase of *Candida albicans* and *Aspergillus*

fumigatus and insights into the enzyme−substrate interactions. *J. Biomol. Struct. Dyn.* **2004**, *22*, 91−99.
(16) Holtje, H. D.; Fattorusso, C. Construction of a model of the *Candida albicans* lanosterol 14-alpha-demethylase active site using the homology modelling technique. *Pharm. Acta Helv.* **1998**, *72*, 271−277.
(17) Ji, H.; Zhang, W.; Zhou, Y.; Zhang, M.; Zhu, J.; Song, Y.; Lü, J.; Zhu, J. A three-dimensional model of lanosterol 14alpha-demethylase of *Candida albicans* and its interaction with azole antifungals. *J. Med. Chem.* **2000**, *43*, 2493−2505.
(18) Lewis, D. F. V.; Wiseman, A.; Tarbit, M. H. Molecular modelling of lanosterol 14 alpha-demethylase (CYP51) from *Saccharomyces cerevisiae* via homology with CYP102, a unique bacterial cytochrome P450 isoform: quantitative structure−activity relationships (QSARs) within two related series of antifungal azole derivatives. *J. Enzyme Inhib.* **1999**, *14*, 175−192.
(19) Talele, T. T.; Hariprasad, V.; Kulkarni, V. M. Docking analysis of Series of Cytochrome P-450 51 DM Inhibiting Azole Antifungals. *Drug Des. Discovery* **1998**, *115*, 181−190.
(20) Gollapudy, R.; Ajmani, S.; Kulkarni, S. A.Modelling and interactions of *Aspergillus fumigatus* lanosterol 14-α demethylase 'A' with azole antifungals. *Bioorg. Med. Chem.* **2004**, *12*, 2937−2750.
(21) Sippl, W.; Contreras, J. M.; Parrot, I.; Rival, Y. M.; Wermuth, C. G. Structure-based 3D QSAR and design of novel acetyl cholinesterase inhibitors. *J. Comput.-Aided. Mol. Des.* **2001**, *15*, 395−410.
(22) Liu, G.; Zhang, Z.; Luo, X.; Shen, J.; Liu, H.; Shen, X.; Chen, K.; Jiang, H. Inhibitory mode of indole-2-carboxamide derivatives against HLGPa: molecular docking and 3D-QSAR analyses. *Bioorg. Med. Chem.* **2004**, *12*, 4147−4157.
(23) Konosu, T.; Tajima, Y.; Takeda, N.; Miyaoka, T.; Kasahara, M.; Yasuda, H.; Oida, S. Triazole antifungals. IV. Synthesis and antifungal activities of 3-acylamino-2-aryl-2-butanol derivatives. *Chem. Pharm. Bull.* **1991**, *39*, 2581−2589.
(24) HyperChem, Hypercube, Inc. 1115 NW 4th Street, Gainesville, FL 32601 U.S.A.
(25) Dewar, M. J. S.; Zoebisch, E. G.; Healy, E. F.; Stewart, J. J. P. AM1: A New General Purpose Quantum Mechanical Molecular model. *J. Am. Chem. Soc.* **1985**, *107*, 3902−3909.
(26) Chem-X July 1999, Chemical Design Ltd. Roundway House, Cromwell Parek, Chipping Norton, Oxfordskire OX 75 SR, U.K.
(27) Vanden Bossche, H.; Koymans, L. Cytochromes P450 in fungi. *Mycoses* **1998**, *41*, 32−8.
(28) Bargar, T. M.; Secor, J.; Markley, L. D.; Shaw, B. A.; Erikson, J. A. A comparative molecular field analysis study of obtusfoliol 14a-methyl demethylase inhibitors. *Pestic. Sci.* **1999**, *44*, 1059−1069.
(29) Tafi, A.; Anastassopoulon, J.; Theophanides, T.; Botta, M.; Corelli, F.; Massa, S.; Artico, M.; Costi, R.; Di Santo, R.; Ragno, R. Molecular modelling of azole antifungal agents active against *Candida albicans*. 1. A comparative molecular field analysis study. *J. Med. Chem.* **1996**, *39*, 1227−1235.
(30) Ferro, D. R.; Hermans, J. A different best rigid-body molecular fit routine. *Acta Crystallogr.* **1977**, *A33*, 345−347.
(31) Dunn, N. J., III; Wold, S.; Edlund, U.; Hellbergo, S.; Gasteiger, J. Multivariate Structure−Activity Relationships between Data from a Battery of Biological Tests and an Ensemble of Structure Descriptors: The PLS Method. *Quant. Struct.-Act. Relat.* **1984**, *3*, 131−137.
(32) Recanatini, M.; Cavalli, A. Comparative Molecular Field Analysis of nonsteroidal aromatase inhibitors: an extended model for two different structural classes. *Bioorg. Med. Chem.* **1998**, *6*, 377−388.
(33) Edlind, T.; Henry, K.; Metera, K.; Katiyar, S. *Aspergillus fumigatus* CYP51 sequence: potential basis for fluconazole resistance. *Med. Mycol.* **2001**, *39*, 299−302.
(34) Podust, L. M.; Poulos, T. L.; Wateman, M. Crystal structure of cytochrome P450 14-sterol demethylase (CYP51) from *Mycobacterium tuberculosis* in complex with azole inhibitors. *Proc. Natl. Acad. Sci. U.S.A.* **2001**, *98*, 3068−3073.
(35) Ravichandran, K. G.; Boddupalli, S.; Haseman, C.; Peterson, J.; Deisenhofer, J. Atomic Structure of the Hemoprotein Domain of Cytochrome P450BM-3: A Prototype for Eukaryotic Microsomal P450s. *Science* **1993**, *261*, 731−736.
(36) Cornell, W. D.; Cieplak, P.; Bayey, C. I.; Gould, I.; Merz, T. K. M.; Ferguson, D. M.; Spellmeyr, D.; Fox, T.; Caldmell, J. W.; Kollman, P. A. Second Generation Force Field for the Simulation of Proteins, Nucleic Acids, and Organic Molecules. *J. Am. Chem. Soc.* **1995**, *117*, 5179−5197.
(37) Gasteiger, J.; Marsili, M. Iterative Partial Equalization of Orbital Electronegativity−A Rapid Access to Atomic Charges. *Tetrahedron* **1980**, *36*, 3219−3228.
(38) Raag, R.; Li, H.; Jones, B.; Poulos, T. Inhibitor-induced conformational change in cytochrome P450cam. *Biochemistry* **1993**, *32*, 4571−4578.
(39) Pajeva, I.; Wiese, M. Molecular modeling of phenothiazines and related drugs as multidrug resistance modifiers: a comparative molecular field analysis. *J. Med. Chem.* **1998**, *41*, 1815−1826.
(40) Sadler, B. R.; Cho, S. J.; Ishaq, K. S.; Chae, K.; Koraeh, K. S. Three-dimensional quantitative structure−activity relationship study of nonsteroidal estrogen receptor ligands using the comparative molecular field analysis/cross-validated r2-guided region selection approach. *J. Med. Chem.* **1998**, *41*, 2261−2267.
(41) Vanden Bossche, H.; Willemsens, G.; Marichal, P.; Cools, W.; Lauwers, W. In *Mode of Action of Antifungal Agents, Ch.5;* Trinci, A. P. J., Ryley, J. F., Eds.; British Mycological Society: London, 1984; pp 321−341.
(42) Vanden Bossche, H.; Marichal, P.; Gorrens, J.; Bellens, D.; Verhoeven, H. D.; Coene, M. C.; Lauwers, W. F.; Janssen, P. A. J. Interaction of azole derivatives with cytochrome P450 isozymes in yeast, fungi and mammalian cells. *Pestic. Sci.* **1987**, *21*, 289−306.
(43) Vanden Bossche, H.; Willemsens, G.; Bellens, D.; Roels, J.; Janssen, P. A. J. From 14 alpha-demethylase inhibitors in fungal cells to androgen and oestrogen biosynthesis inhibitors in mammalian cells. *Biochem. Soc. Trans.* **1990**, *18*, 10−13.
(44) Marichal, P.; Koymans, L.; Willemsens, S.; Bellens, D.; Verhasselt, P.; Luyten, W.; Borgers, M.; Ramaekers, F. C.; Odds, F. C.; Bossche, H. V. Contribution of mutations in the cytochrome P450 14{alpha}-demethylase (Erg11p, Cyp51p) to azole resistance in *Candida albicans*. *Microbiology* **1999**, *145*, 2701−2713.
(45) Sanglard, D.; Ischer, F.; Koymans, L.; Bille, J. Amino Acid Substitutions in the Cytochrome P-450 Lanosterol 14alpha-Demethylase (CYP51A1) from Azole-Resistant *Candida albicans* Clinical Isolates Contribute to Resistance to Azole Antifungal Agents. *Antimicrob. Agents Chemother.* **1998**, *42*, 241−253.
(46) Lamb, D. C.; Kelly, D. E.; Schunck, W. H.; Shyadehi, A. Z.; Akhtar, M.; Lowe, D. J.; Baldwin, B. C.; Kelly, S. L. The mutation T315A in *Candida albicans* sterol 14α-demethylase causes reduced enzyme activity and fluconazole resistance through reduced affinity. *J. Biol. Chem.* **1997**, *272*, 5682−5688.
(47) Asai, K.; Tsuchimori, N.; Okonogi, Ko.; Peofeet, J. R.; Gotob, O.; Yoshida, Y. Formation of Azole-Resistant *Candida albicans* by Mutation of Sterol 14-Demethylase P450. *Antimicrob. Agents Chemother.* **1999**, *43*, 1163−1169.
(48) Kelly, S. L.; Lamb, D. C.; Kelly, D. E. Molecular analysis of cyp51 from fluconazole-resistant *Candida albicans* strains. *FEMS Microbiol. Lett.* **1999**, *180*, 171−175.
(49) White, T. C. Increased mRNA levels of ERG16, CDR, and MDR1 correlate with increases in azole resistance in *Candida albicans* isolates from a patient infected with human immunodeficiency virus. *Antimicrob. Agents Chemother.* **1997**, *41*, 1488−1494.
(50) Klopman, G.; Ptchelintsev, D. J. Antifungal triazole alcohols: a comparative analysis of structure−activity, structure-teratogenicity and structure-therapeutic index relationships using the Multiple Computer-Automated Structure Evaluation (Multi-CASE) methodology. *J. Comput.-Aided Mol. Des.* **1993**, *7*, 349−362.
(51) Talele, T. T.; Kulkarni, V. M. Three-dimensional quantitative structure−activity relationship (QSAR) and receptor mapping of cytochrome P-450 (14 alpha DM) inhibiting azole antifungal agents. *J. Chem. Inf. Comput. Sci.* **1999**, *39*, 204−210.
(52) Lewis, D. F. V.; Parke, I. D. V. Molecular modelling of cytochrome CYP1A1: a putative access channel explains differences in induction potency between the isomers benzo[*a*] pyrene and benzo[*e*]pyrene, and 2- and 4-acetylaminofluorene. *Toxicol. Lett.* **1994**, *71*, 235−243.
(53) Kelly, S. L.; Lamb, D. C.; Kelly, D. E.; Manning, N. J.; Loeffler, J.; Hebart, H.; Schumacher, U.; Einsele, H. Resistance to fluconazole and cross-resistance to amphotericin B in *Candida albicans* from AIDS patients caused by defective sterol delta5,6-desaturation. *FEBS Lett.* **1997**, *400*, 80−2.
(54) Cupp-Vickery, J. R.; Garcia, C.; Hofacre, A.; McGee-estrada, K.; CuppVickery, J. R.; Garcia, C.; Hofacre, A.; McGee-estrada, K. Ketoconazole-induced conformational changes in the active site of cytochrome P450eryF. *J. Mol. Biol.* **2001**, *311*, 101−110.
(55) Xiao, L.; Madison, V.; Chau, A. S.; Loebenberg, D.; Palermo, R. E.; McNicholas, P. M. Three-dimensional models of wild-type and mutated forms of cytochrome P450 14α-sterol demethylases from *Aspergillus fumigatus* and *Candida albicans* provide insights into posaconazole binding. *Antimicrob. Agents Chemother.* **2004**, *48*, 568−574.
(56) Kim, K. H. In *3D QSAR in Drug Design: Recent Advances*; Kubinyi, M., Folkers, G., Martin, Y. C., Eds.; Kluwer/E SCOM: London, 1998; pp 233−255.
(57) Cavalli, A.; Greco, G.; Novelliono, E.; Recanatini, M. Linking 3D-QSAR and protein homology models of enzyme−inhibitor interactions: an application to nonsteroidal aromatase inhibitors. *Bioorg. Med. Chem.* **2000**, *8*, 2771−2780.

CI0496494